

# Vision-Based Object Detection for UAV Solar Panel Inspection Using an Enhanced Defects Dataset

Ashen Rodrigo<sup>1</sup>, Isuru Munasinghe<sup>2</sup>, Asanka Perera<sup>3</sup>

<sup>1</sup>Department of Electrical Engineering, University of Moratuwa, Katubedda, Sri Lanka

<sup>2</sup>Department of Electronic and Telecommunication Engineering, University of Moratuwa, Katubedda, Sri Lanka

<sup>3</sup>School of Engineering, University of Southern Queensland, Brisbane, Australia

**Abstract**—Timely and accurate detection of defects and contaminants in solar panels is critical for maintaining the efficiency and reliability of photovoltaic systems. This study presents a comprehensive evaluation of five state-of-the-art object detection models: YOLOv3, Faster R-CNN, RetinaNet, EfficientDet, and Swin Transformer, for identifying physical and electrical defects as well as surface contaminants such as dust, dirt, and bird droppings on solar panels. A custom dataset, annotated in the COCO format and specifically designed for solar panel defect and contamination detection, was developed alongside a user interface to train and evaluate the models. The performance of each model is assessed and compared based on mean Average Precision (mAP), precision, recall, and inference speed. The results demonstrate the trade-offs between detection accuracy and computational efficiency, highlighting the relative strengths and limitations of each model. These findings provide valuable guidance for selecting appropriate detection approaches in practical solar panel monitoring and maintenance scenarios.

The dataset will be publicly available in [1].

**Index Terms**—solar panel inspection, defect detection, deep learning, object detection models, UAV-based monitoring

## I. INTRODUCTION

The efficiency of photovoltaic (PV) systems is highly dependent on the cleanliness and structural integrity of the solar panels. Accumulation of dust, dirt, and bird droppings can reduce energy conversion efficiency by up to 80%, while undetected physical or electrical damage may lead to long-term degradation and safety risks [2], [3]. Traditional manual cleaning and even most existing robotic cleaning systems lack the capability to assess the actual contamination or defect levels on the panels [4]–[7]. Instead, they perform uniform cleaning across the entire surface without distinguishing between clean and contaminated regions. This approach not only leads to excessive consumption of water and electrical power but also introduces unnecessary mechanical stress on panels, which can exacerbate existing micro-cracks or electrical faults.

To address these limitations, we propose an approach that integrates intelligent detection with targeted cleaning strategies. UAV-based inspection enables the rapid identification of contaminated areas and the isolation of physically or electrically damaged panels before cleaning, ensuring maintenance efficiency and preventing further damage. Once contamination is detected, UGVs or robotic cleaning units can selectively clean only the affected regions, avoiding panels that require repair. This proposed method reduces resource usage and

operational costs while maximizing PV system output, as illustrated in Fig. 1.

Deep learning-based object detection models are pivotal in enabling automated identification of surface contaminants such as dust and bird droppings, as well as physical and electrical defects on solar panels [8]. Utilizing UAV imagery with advanced detection algorithms enables the creation of maintenance maps for UGVs, supporting efficient and safe operation of PV systems. However, a significant challenge in this field is the limited availability of publicly accessible, well-annotated, and class-balanced solar panel defect datasets, which hinders the development and training of accurate detection models.

In summary, the contributions of this paper are as follows:

- 1) We publish an enhanced solar panel defect detection dataset by augmenting an existing publicly available dataset with additional class-specific images.
- 2) We benchmark five state-of-the-art object detection architectures using the proposed dataset, providing a performance evaluation.
- 3) We conduct a comparative analysis of model performance on the improved dataset and the original publicly available dataset, highlighting the impact of the proposed enhancements.

This paper is organized as follows: Section II presents the related work, Section III details the proposed methodology and experimental setup, Section IV presents and analyzes

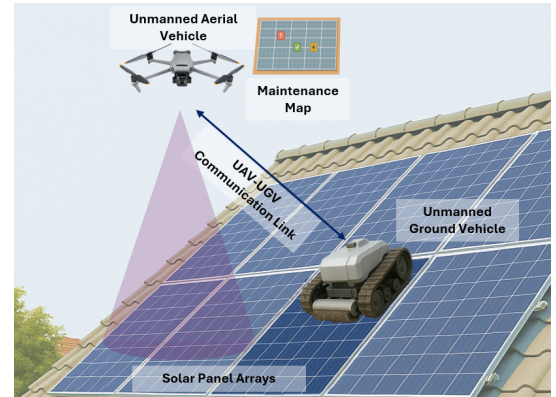


Fig. 1. UAV-Assisted Solar Panel Maintenance Guiding UGVs for Targeted Cleaning.

the results, and Section V summarizes the contributions and discusses future research directions.

## II. LITERATURE REVIEW

Several approaches have been proposed for the detection of dirt on solar panels, containing both sensor-based and vision-based methodologies. Weight sensor systems have been utilized to initiate cleaning when dust accumulation causes the weight of the panel to exceed predefined thresholds. However, these systems can be susceptible to environmental vibrations and structural load variations, potentially affecting accuracy [9]. Radiometric sensor-based UAV platforms have employed thermal emissivity analysis for contamination detection with high reported accuracy, although their performance may be influenced by ambient temperature and humidity fluctuations [10]. In [11], multi-sensor prototypes integrating illuminance, voltage, current, temperature, humidity, and dust density measurements were developed to determine cleaning schedules. Nevertheless, these solutions face challenges related to sensor calibration stability and long-term operational reliability.

Vision-based methods for solar panel inspection have utilized RGB-infrared smart camera systems with real-time image processing to enable autonomous detection and cleaning operations [12], [13]. These systems can continuously capture and analyze panel imagery, facilitating timely maintenance decisions without manual intervention. Multi-sensor fusion techniques that integrate thermal and visible-light imaging have also been applied for simultaneous hotspot identification and contaminant detection, providing a more comprehensive assessment of panel health [14]. In addition, texture analysis approaches, such as those employing Gray Level Co-occurrence Matrix (GLCM) features with contrast-enhancing pre-processing, have achieved high recognition accuracy in controlled environments, enabling effective classification of dirt and soil on panel surfaces [15].

In [16], image processing was combined with dust sensors and irradiance data to estimate panel voltage using a neural network model, enabling automated cleaning triggers when output dropped below a predefined threshold. The work in [17] proposed a fast self-adaptive computer vision method with a dust detection camera and machine learning models to classify clean and dusty panels. In [18], a comparative analysis of ANN, Multi-Layer Perceptron, and DenseNet architectures for image-based dust detection showed DenseNet achieving the highest accuracy of 98%. The study in [19] used drone-acquired high-resolution imagery and MATLAB-based algorithms to assess dust accumulation, validated against electrical measurements with minimal variation. In [20], image processing outputs were integrated with ANN, LSTM, and SVR models to predict solar panel performance under varying environmental conditions. However, the reliability of image processing thresholding methods may be adversely affected by variations in illumination, occlusions, and environmental conditions encountered in real-world scenarios.

## III. METHODOLOGY

This section describes the datasets, data preprocessing, model selection, training procedures, and evaluation metrics used in this study.

### A. Datasets

The evaluation of the object detection models was conducted using two distinct datasets to ensure a comprehensive assessment under diverse operational conditions. Both datasets were employed for training and validation to facilitate a comparative analysis of model performance across different data distributions.

- Roboflow Dataset [21]: A publicly available dataset containing solar panel images annotated for multiple defect categories, including cracks, bird droppings, dust accumulation, and electrical hotspots. While it provides a broad range of examples suitable for initial benchmarking, the dataset exhibits a pronounced class imbalance, which can adversely affect the detection accuracy for underrepresented defect types.
- Our Customized Dataset [1]: A balanced dataset was constructed to address the class imbalance present in the original data. As shown in Fig. 2, the initial dataset exhibited greater confusion in classes with fewer samples compared to those with larger sample sizes. To mitigate this, the Roboflow dataset was restructured to contain 190 images per class. For classes with fewer original samples, data augmentation techniques were applied to achieve the desired count. The resulting dataset was subsequently partitioned into training, validation, and test subsets. This balanced configuration allows for a more uniform distribution of confusion across all classes.

Although data augmentation helps increase sample size for underrepresented classes, it is preferable to rely primarily on raw, original data to preserve the natural variability and authenticity of the dataset. Excessive augmentation, especially increasing samples up to 300 or more, risks degrading dataset quality by over-representing artificially modified images. This may cause models to learn less generalizable features, ultimately reducing performance on real-world data. Besides augmentation, methods such as collecting additional raw data, applying class-weighted loss functions, or using advanced sampling strategies can be used to maintain both dataset integrity and model robustness to address class imbalance effectively.

Both datasets were used for training and performance evaluation of the object detection models, enabling a comparison under imbalanced and balanced data distributions.

### B. Class Definitions and Distribution

The defect detection task comprises five primary classes, each representing a distinct condition with the potential to affect the operational efficiency and reliability of PV systems:

- 1) Bird Drop: Localized organic contamination caused by bird droppings, which can induce partial shading, reduce

power output, and potentially lead to hotspot formation due to uneven irradiation.

- 2) Clean: Panels free from visible defects or surface contamination, serving as the baseline condition for comparison in defect detection and classification tasks.
- 3) Dusty: Accumulated particulate matter such as dust, which obstructs light transmission and can cause substantial efficiency reduction if not removed in a timely manner.
- 4) Electrical: Localized heating zones or discolorations caused by electrical faults or shading anomalies, often serving as early indicators of performance degradation or imminent panel failure.
- 5) Physical: Structural damage or surface anomalies, including cracks, scratches, or deformation, that may compromise panel integrity.

Table I presents the image distribution per class across the training, validation, and test splits for both the original (unbalanced) Roboflow dataset and the custom balanced dataset. The balanced dataset was created by selecting images common across classes and equalizing the number of images to 140 per class for training, 30 for validation, and 20 for testing.

TABLE I  
IMAGE DISTRIBUTION PER CLASS FOR ORIGINAL (UNBALANCED) AND CUSTOM BALANCED DATASETS.

Class	Original Dataset			Balanced Dataset		
	Train	Validation	Test	Train	Validation	Test
Bird Drop	336	31	16	140	30	20
Clean	402	41	18	140	30	20
Dusty	366	33	18	140	30	20
Electrical	180	19	12	140	30	20
Physical	146	12	3	140	30	20

### C. Data Preprocessing and Augmentation

All images and corresponding annotations were standardized to the COCO format, which is a widely adopted benchmark in object detection tasks. Model generalization and overfitting mitigation were enhanced through the application of several data augmentation strategies during training. The augmentation pipeline incorporated random horizontal and vertical flipping, variable-angle rotation, brightness and contrast adjustments using color jittering, and adaptive scaling with cropping to align with the input resolution requirements of each model. These augmentation techniques replicate real-world variability in solar panel imagery resulting from fluctuations in illumination, changes in camera perspective, and diverse environmental conditions by improving the generalization capabilities of the models.

### D. Benchmark Model Selection and Transfer Learning Framework

Five state-of-the-art object detection architectures were employed to establish a benchmarking framework, namely YOLOv3 [22], Faster R-CNN [23], RetinaNet [24], EfficientDet [25], and the Swin Transformer [26]. These models

represent the two principal object detection paradigms. Single-stage detectors, demonstrated by YOLOv3, RetinaNet, and EfficientDet, conduct classification and localization in a single forward pass, enabling high inference speeds. In contrast, two-stage detectors, such as Faster R-CNN, first generate a set of candidate object proposals and subsequently refine these through dedicated classification and bounding box regression stages, often achieving higher detection accuracy at the cost of increased computational demand.

From an architectural perspective, the selected models encompass a broad range of design principles. YOLOv3 employs the Darknet-53 convolutional backbone, while Faster R-CNN and RetinaNet utilize ResNet-based Feature Pyramid Networks to enhance multi-scale feature representation. EfficientDet includes a compound scaling strategy and a Bi-directional Feature Pyramid Network for improved efficiency and accuracy balance. The Swin Transformer introduces a hierarchical vision transformer backbone with shifted window-based self-attention, enabling long-range dependency modeling while preserving computational efficiency. This architectural diversity facilitates a comparative evaluation in terms of detection accuracy, computational complexity, and inference latency.

All models were initialized with weights pre-trained on the COCO dataset and subsequently fine-tuned on the solar panel datasets using a transfer learning approach. Utilizing pre-trained weights allowed the architectures to inherit high-level feature representations obtained from large-scale object detection tasks, which accelerated convergence, reduced training time, and improved overall performance under limited domain-specific data availability.

### E. Training Setup

Transfer learning was implemented using the MMDetection framework, with all models fine-tuned on the solar panel defect datasets. For each experiment, models were trained independently on both the original (unbalanced) and balanced datasets, initializing from pre-trained weights obtained from large-scale datasets such as COCO. Input images were resized to either  $224 \times 224$  or  $256 \times 256$  pixels in accordance with the respective architectural specifications of the model, and batch sizes were set between 1 and 4, determined by available GPU memory resources. The learning rate was initialized at 0.001 and decayed progressively, with hyperparameters tuned individually for each model to optimize performance.

Training was conducted for a maximum of 100 epochs, with validation performed at 10-epoch intervals to monitor accuracy and loss trends. An early stopping strategy was used to mitigate overfitting, terminating training when no improvement was observed over successive validation cycles. All models were optimized using Stochastic Gradient Descent (SGD) with a momentum coefficient of 0.9 and a weight decay of 0.0001. All experiments were executed on an NVIDIA RTX 3090 GPU within an Ubuntu-based Conda environment.

## F. Evaluation Metrics

The evaluation of the object detection models was conducted using multiple quantitative metrics to assess accuracy, reliability, and computational efficiency. These metrics provide a detailed understanding of the effectiveness of the models for detecting solar panel defects under practical conditions.

- 1) **Mean Average Precision (mAP):** mAP is the primary metric for object detection tasks, combining classification and localization performance. It computes the area under the precision–recall curve for each defect class and averages these values across all classes. Multiple Intersection over Union (IoU) thresholds (0.5 to 0.95) are used to evaluate detection robustness. The mAP is defined as in Eq. 1.

$$mAP = \frac{1}{N} \sum_{i=1}^N \int_0^1 P_i(R) dR \quad (1)$$

where  $P_i(R)$  is the precision as a function of recall for class  $i$ , and  $N$  is the total number of classes.

- 2) **Precision and Recall:** Precision measures the proportion of correctly identified defects among all detections, while recall quantifies the proportion of actual defects correctly detected. Both are defined in Eq. 2.

$$\text{Precision} = \frac{TP}{TP + FP}, \quad \text{Recall} = \frac{TP}{TP + FN} \quad (2)$$

where  $TP$ ,  $FP$ , and  $FN$  denote true positives, false positives, and false negatives, respectively.

- 3) **F1-Score:** The F1-score provides a balanced measure between precision and recall, defined in Eq. 3.

$$F1 = 2 \cdot \frac{\text{Precision} \cdot \text{Recall}}{\text{Precision} + \text{Recall}} \quad (3)$$

- 4) **Inference Speed (Frames Per Second - FPS):** FPS evaluates computational efficiency and determines the model's practicality for real-time applications, such as drone inspections or robotic maintenance. Fast inference is critical when inspecting large solar farms where timely detection impacts operational costs and system uptime. It is calculated as in Eq. 4.

$$FPS = \frac{\text{Number of images processed}}{\text{Inference time (s)}} \quad (4)$$

- 5) **Intersection over Union (IoU):** IoU quantifies localization accuracy by measuring the overlap between predicted and ground-truth bounding boxes, as given in Eq. 5.

$$IoU = \frac{|B_p \cap B_g|}{|B_p \cup B_g|} \quad (5)$$

where  $B_p$  and  $B_g$  are the predicted and ground-truth bounding boxes, respectively.

- 6) **False Positive Rate (FPR) and False Negative Rate (FNR):** FPR and FNR measure incorrect and missed detections relative to total negative and positive instances. These are defined in Eq. 6.

$$FPR = \frac{FP}{FP + TN}, \quad FNR = \frac{FN}{FN + TP} \quad (6)$$

where  $TN$  represents true negatives.

- 7) **Average Recall (AR):** AR computes the mean recall across multiple IoU thresholds and detection limits, as shown in Eq. 7.

$$AR = \frac{1}{K} \sum_{k=1}^K \text{Recall}(IoU_k) \quad (7)$$

where  $K$  is the number of IoU thresholds evaluated.

- 8) **Confusion Matrix and Per-Class Metrics:** The confusion matrix provides the distribution of predictions across true and predicted classes, enabling per-class evaluation of precision, recall, and IoU to identify weaknesses for specific defect types.

The selection of mAP, precision, recall, and inference speed as the primary evaluation metrics is determined by the operational and methodological requirements of automated solar panel defect detection systems. mAP as defined in Eq. 1, provides a comprehensive measure of both classification fidelity and localization accuracy across all defect categories, making it the standard metric for benchmarking object detection models. Precision and recall address critical operational needs by balancing the minimization of false alarms against the requirement for exhaustive defect coverage.

Inference speed, expressed in frames per second, directly reflects the feasibility of deploying these models in real-time UAV-assisted inspection workflows, where timely anomaly detection is essential for large-scale PV maintenance. Supplementary metrics, including the F1-score, IoU, and error-based measures such as FPR and FNR, provide additional insight into sensitivity–specificity trade-offs and spatial localization quality. The use of confusion matrices and per-class analyses enables a granular understanding of model behavior across different defect types, which is particularly important given the heterogeneous nature and varying operational impact of cracks, surface contamination, and electrical faults.

It is important to note that the balanced dataset contains a significantly reduced number of training images compared to the original dataset. This reduction inevitably leads to lower precision, recall, and overall F1 scores across all models due to the decreased sample diversity. However, as observed in the corresponding confusion matrices, the class-wise confusion is significantly reduced in the balanced dataset results, indicating that the models are better at distinguishing between defect classes despite the lower overall metrics.

## IV. EXPERIMENTAL RESULTS AND ANALYSIS

This section presents the quantitative evaluation results of five state-of-the-art object detection models for solar panel defect detection, comparing performance on the original imbalanced dataset and a custom balanced dataset.

### A. Model Performance

As presented in Table II, the Swin Transformer demonstrated the highest overall detection performance across both datasets, achieving precision, recall, F1 score, and mAP values

TABLE II  
PERFORMANCE COMPARISON OF DETECTION MODELS ON ORIGINAL AND BALANCED DATASETS.

Model	Original (Unbalanced) Dataset					Balanced Dataset				
	Precision	Recall	F1 Score	mAP	FPS	Precision	Recall	F1 Score	mAP	FPS
YOLOv3	0.76	0.79	0.77	0.77	45	0.68	0.71	0.69	0.70	30
Faster R-CNN	0.81	0.83	0.82	0.79	8	0.73	0.75	0.74	0.74	5
RetinaNet	0.75	0.78	0.76	0.75	20	0.67	0.70	0.68	0.69	14
EfficientDet	0.83	0.85	0.84	0.83	25	0.74	0.76	0.75	0.75	17
Swin Transformer	0.88	0.85	0.86	0.87	12	0.80	0.78	0.79	0.80	8

of 0.88, 0.85, 0.86, and 0.87, respectively, on the original dataset, and maintaining competitive results on the balanced dataset despite the reduced training sample size. EfficientDet also exhibited strong accuracy while offering comparatively higher inference speed, making it a feasible option where computational efficiency is a priority. In contrast, YOLOv3 achieved the highest inference speed but with lower precision and recall, reflecting a trade-off between rapid processing and detection accuracy. The observed decline in performance metrics for all models on the balanced dataset can be attributed to the reduced sample diversity. However, the improved class balance enhanced defect-type separability, particularly for underrepresented categories such as physical and electrical faults, by reducing class-specific misclassification.

### B. Combined Confusion Matrices for All Models

The combined confusion matrices in Fig. 2 illustrate the trade-off between overall detection accuracy and class-wise separability when transitioning from the original imbalanced dataset to the balanced dataset. In the original dataset, higher aggregate metrics were observed, with YOLOv3 correctly classifying 336 “Clean” samples and the Swin Transformer accurately detecting 343 “Dusty” samples, although substantial misclassification persisted in minority classes, with Physical defects frequently misidentified as Clean or Dusty (e.g., YOLOv3 misclassifying 27 Physical samples as Bird Drop). Following dataset balancing, the detection of minority classes improved, with the Swin Transformer increasing correct classifications of Physical defects from 134 to 170 and Electrical defects from 168 to 172, while YOLOv3 improved Physical defect recognition from 116 to 151. These gains were accompanied by a modest reduction in majority-class performance, attributable to the smaller and less diverse training set. Overall, the Swin Transformer consistently achieved the most balanced performance, maintaining strong detection rates for the majority classes while delivering the most substantial relative improvement in minority-class recognition after balancing.

### C. Interference Images per Class in One Row

Fig. 3 presents representative interference visualizations for each defect class in the solar panel dataset, with ground truth annotations shown in green and model predictions in blue. The examples illustrate the ability of the model to accurately localize and classify diverse defect types, including scenarios where more than one defect type is present. The close alignment between predicted and ground truth boundaries in most cases demonstrates precise spatial localization, while the

presence of multiple bounding boxes highlights the potential for detecting complex defect scenarios that may require post-processing or filtering in operational deployment.

## V. CONCLUSION

This research presented a comprehensive benchmark of five state-of-the-art deep learning-based object detection models for real-time solar panel defect detection, using both an existing imbalanced dataset and a custom balanced dataset augmented with synthetic samples. The results demonstrated that the Swin Transformer achieved the highest performance across all evaluation metrics on both datasets, recording a precision of 0.88 and 0.90, recall of 0.85 and 0.88, F1-score of 0.86 and 0.89, and mAP of 0.87 and 0.88, while maintaining an inference speed of twelve frames per second. These results



Fig. 2. Combined Confusion Matrices for All Evaluated Models, with the Left Column Showing Results on the Original (Unbalanced) Dataset and the Right Column Showing Results on the Balanced Dataset.



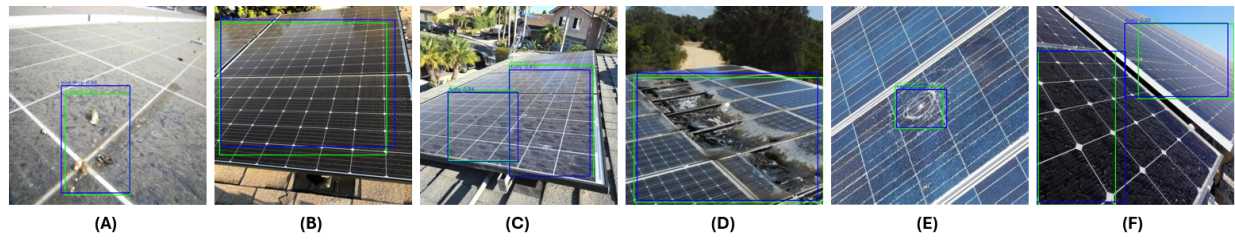


Fig. 3. Side-by-Side Interference Visualizations for Solar Panel Defect Classes Generated by the Swin Transformer. Ground Truth Bounding Boxes Are Shown in Green and Perturbed Predictions in Blue. (A) Bird Dropping, (B) Clean, (C) Dusty, (D) Electrical, (E) Physical, (F) Multi-Class (Clean and Dusty).

highlight the capability of the model to deliver high detection accuracy while maintaining practical real-time applicability, making it a strong candidate for UAV-assisted PV inspection and maintenance operations. The key contribution of the study lies in providing a comparative evaluation of leading object detection architectures under balanced and imbalanced data conditions, by offering actionable insights for selecting optimal models in operational environments.

Future work will focus on optimizing the model for deployment on UAV-mounted edge devices, enabling low-latency, in-flight inference for efficient large-scale solar farm inspections.

## REFERENCES

- [1] A. Rodrigo, I. Munasinghe, and A. Perera, "Solar panel inspection dataset," <https://github.com/IsuruMunasinghe98/solar-panel-inspection-dataset>, 2025.
- [2] P. Patil, J. Bagi, and M. Wagh, "A review on cleaning mechanism of solar photovoltaic panel," in *2017 International Conference on Energy, Communication, Data Analytics and Soft Computing (ICECDS)*. IEEE, 2017, pp. 250–256.
- [3] A. Sayyah, M. N. Horenstein, and M. K. Mazumder, "Energy yield loss caused by dust deposition on photovoltaic panels," *Solar Energy*, vol. 107, pp. 576–604, 2014.
- [4] I. Munasinghe, V. Vijenayake, S. Viduranga, Y. Lokugama, and P. Jayasekara, "Design and implementation of a semi-autonomous robotic system for systematic solar panel cleaning," in *2024 9th International Conference on Control and Robotics Engineering (ICCRE)*. IEEE, 2024, pp. 61–67.
- [5] K. Jaiganesh, K. B. S. Reddy, B. Shobhitha, and B. D. Goud, "Enhancing the efficiency of rooftop solar photovoltaic panel with simple cleaning mechanism," *Materials Today: Proceedings*, vol. 51, pp. 411–415, 2022.
- [6] I. Munasinghe, V. Vijenayake, and P. Jayasekara, "Improving Navigation of a Semi-Autonomous Solar Panel Cleaning Robot through Advanced Localization and Edge Detection," *International Journal of Science Engineering and Management (IJSEM)*, vol. 12, no. 1, Jan. 2025.
- [7] B. O. Olorunfemi, O. A. Ogbolumani, and N. Nwulu, "Solar panels dirt monitoring and cleaning for performance improvement: a systematic review on smart systems," *Sustainability*, vol. 14, no. 17, p. 10920, 2022.
- [8] F. Sun, C. Yang, H. Cui, Z. Lv, J. Shao, B. Zhao, and K. He, "Dust Detection Techniques for Photovoltaic Panels from a Machine Vision Perspective: A Review," in *2023 8th Asia Conference on Power and Electrical Engineering (ACPEE)*. IEEE, 2023, pp. 1413–1418.
- [9] N. Ronnaronglit and N. Maneerat, "A cleaning robot for solar panels," in *2019 5th International Conference on Engineering, Applied Sciences and Technology (ICEAST)*. IEEE, 2019, pp. 1–4.
- [10] F. P. G. Márquez and I. S. Ramírez, "Condition monitoring system for solar power plants with radiometric and thermographic sensors embedded in unmanned aerial vehicles," *Measurement*, vol. 139, pp. 152–162, 2019.
- [11] N. Khadka, A. Bista, B. Adhikari, A. Shrestha, and D. Bista, "Smart solar photovoltaic panel cleaning system," in *IOP Conference Series: Earth and Environmental Science*, vol. 463, no. 1. IOP Publishing, 2020, p. 012121.
- [12] E. Yfantis and A. Fayed, "A camera system for detecting dust and other deposits on solar panels," *Advances in Image and Video Processing*, vol. 2, no. 5, pp. 1–10, 2014.
- [13] L. A. Zadeh, "Fuzzy sets," *Information and control*, vol. 8, no. 3, pp. 338–353, 1965.
- [14] Z. He, Y. Zhang, and H. Li, "Self-inspection cleaning device for photovoltaic power plant based on machine vision," in *IOP Conference Series: Earth and Environmental Science*, vol. 242. IOP Publishing, 2019, p. 032020.
- [15] K. A. Abuqaoud and A. Ferrah, "A novel technique for detecting and monitoring dust and soil on solar photovoltaic panel," in *2020 Advances in Science and Engineering Technology International Conferences (ASET)*. IEEE, 2020, pp. 1–6.
- [16] D. Saquib, M. N. Nasser, and S. Ramaswamy, "Image Processing Based Dust Detection and prediction of Power using ANN in PV systems," in *2020 Third International Conference on Smart Systems and Inventive Technology (ICSSIT)*. IEEE, 2020, pp. 1286–1292.
- [17] N. N. Karima, K. Rimon, M. S. Molla, M. Hasan, and M. H. Bhuyan, "Advanced image processing based solar panel dust detection system," in *2023 26th International Conference on Computer and Information Technology (ICCIT)*. IEEE, 2023, pp. 1–6.
- [18] S. Keerthana, S. Hariharasudhan *et al.*, "Image processing-based dust detection for solar panels," in *2024 International Conference on Smart Systems for Electrical, Electronics, Communication and Computer Engineering (ICSSECC)*. IEEE, 2024, pp. 511–515.
- [19] H. Qasem, A. Mnatsakanyan, and P. Banda, "Assessing dust on pv modules using image processing techniques," in *2016 IEEE 43rd Photovoltaic Specialists Conference (PVSC)*. IEEE, 2016, pp. 2066–2070.
- [20] M. Mamdouh and Y. A. Zaghloul, "Fusion between image processing and machine learning for dust detection on solar panels," in *2024 Fifteenth International Conference on Ubiquitous and Future Networks (ICUFN)*. IEEE, 2024, pp. 169–174.
- [21] solarpaneldataset, "solarpanel Dataset," <https://universe.roboflow.com/solarpaneldataset/solarpanel-ggmm>, Feb. 2025.
- [22] J. Redmon and A. Farhadi, "YOLOv3: An Incremental Improvement," *arXiv preprint arXiv:1804.02767*, 2018.
- [23] S. Ren, K. He, R. Girshick, and J. Sun, "Faster R-CNN: Towards Real-Time Object Detection with Region Proposal Networks," *IEEE Transactions on Pattern Analysis and Machine Intelligence*, vol. 39, no. 6, pp. 1137–1149, 2017.
- [24] T.-Y. Lin, P. Goyal, R. Girshick, K. He, and P. Dollár, "Focal Loss for Dense Object Detection," in *Proceedings of the IEEE International Conference on Computer Vision (ICCV)*, 2017, pp. 2980–2988.
- [25] M. Tan, R. Pang, and Q. V. Le, "EfficientDet: Scalable and Efficient Object Detection," in *Proceedings of the IEEE/CVF Conference on Computer Vision and Pattern Recognition (CVPR)*, 2020, pp. 10778–10787.
- [26] Z. Liu, Y. Lin, Y. Cao, H. Hu, Y. Wei, Z. Zhang, S. Lin, and B. Guo, "Swin Transformer: Hierarchical Vision Transformer using Shifted Windows," in *Proceedings of the IEEE International Conference on Computer Vision (ICCV)*, 2021, pp. 10012–10022.